JGR Oceans

RESEARCH ARTICLE

10.1029/2025JC022384

The Limits of Ocean Forcing on the Exchange Flow of the Salish Sea

R. Sanchez[1,2], **S. N. Giddings**[2], **and E. Lemagie**[3]

[1]Department of Civil and Coastal Engineering, University of Florida, Gainesville, FL, USA, [2]Scripps Institution of Oceanography, UC San Diego, San Diego, CA, USA, [3]NOAA Pacific Marine Environmental Laboratory, Seattle, WA, USA

Key Points:

- Along-shelf winds drive variability of landward salt transport through the Salish Sea until the flow reaches sill-influenced constrictions
- Transient and seasonal ocean forcing are associated with different length scales within the Salish Sea
- Bulk inflowing salinity and outflowing salinity values are useful in distinguishing local versus oceanic control of salt transport

Supporting Information:

Supporting Information may be found in the online version of this article.

Correspondence to:

R. Sanchez,
robert.sanchez@ufl.edu

Citation:

Sanchez, R., Giddings, S. N., & Lemagie, E. (2025). The limits of ocean forcing on the exchange flow of the Salish Sea. *Journal of Geophysical Research: Oceans*, *130*, e2025JC022384. https://doi.org/10.1029/2025JC022384

Received 17 JAN 2025
Accepted 23 APR 2025

Author Contributions:

Conceptualization: S. N. Giddings
Data curation: R. Sanchez, E. Lemagie
Formal analysis: R. Sanchez
Funding acquisition: S. N. Giddings
Investigation: R. Sanchez
Project administration: S. N. Giddings
Supervision: S. N. Giddings, E. Lemagie
Writing – original draft: R. Sanchez
Writing – review & editing: R. Sanchez, S. N. Giddings, E. Lemagie

Abstract The dynamics of ocean-estuary exchange depend on a variety of local and remote ocean forcing mechanisms where local mechanisms include those directly forcing the estuary such as tides, river discharge, and local wind stress; remote forcing includes forcing from the ocean such as coastal wind stress and coastal stratification variability. We use a numerical model to investigate the limits of oceanic influence, such as wind-driven upwelling, on the Salish Sea exchange flow and salt transport. We find that along-shelf winds substantially modulate flow throughout the Strait of Juan de Fuca until flow reaches sill-influenced constrictions. At these constrictions the exchange flow variability becomes sensitive to local tidal and river forcing. The salt exchange variability is tidally dominated at Admiralty Inlet and upwelling has little impact on seasonal salt exchange variability. While within Haro Strait, the salt exchange variability is driven by a mix of coastal upwelling and local forcing including river discharge. There, the transition from oceanic to local control of salt exchange occurs over a longer distance and is primarily identifiable in the increasing variability of bulk outflowing salinity values. The differences between the two locations highlight how ocean variability interacts with both tidal pumping and gravitational circulation. We also distinguish between transient ocean forcing which can modify fjord properties near the mouth of the strait and seasonal ocean forcing which primarily affects along-strait pressure gradients. The results have implications for understanding the transport variability of biogeochemical variables that are influenced by both along-shelf winds and local sources.

Plain Language Summary Over periods of time longer than a day, the circulation of estuaries is generally composed of inflowing salty water at depth and relatively fresh outflowing water near the surface. This pattern of circulation, called the exchange flow, is responsible for replenishing water in an estuary and transporting waterborne material including nutrients, larvae, and pollutants. This circulation is maintained by freshwater from rivers and mixing of fresh and salty water by tides. However, the circulation can also be influenced by changes in ocean conditions. For example, summer coastal wind-driven upwelling can bring dense water into an estuary which increases density gradients and increases the circulation. In this study we use a simulation of the Salish Sea in the Pacific Northwest to quantify how important ocean forcing is in modifying an estuary's circulation. We find that the coastal wind-driven circulation is the most important force modifying circulation until the flow reaches channel constrictions. These results imply that the exchange of nutrients is also dominated by ocean conditions deep into the estuary. At the constrictions, the circulation becomes more sensitive to local factors such as tides and river flow.

1. Introduction

Ocean-estuary exchange impacts biological, chemical, and physical processes in estuaries, such as larval dispersal (e.g., Brasseale et al., 2019), hypoxia (e.g., Adelson et al., 2022), residence time (e.g., Xiong et al., 2021), primary productivity (e.g., Cloern et al., 2014), salinity intrusion (e.g., Payo-Payo et al., 2022), and glacial melt rates (e.g., Bao & Moffat, 2024). Similarly, ocean-estuary exchange can impact coastal ocean biogeochemistry and productivity (e.g., Boyer et al., 2002; Davis et al., 2014), circulation, and transport pathways (e.g., Banas et al., 2009). The magnitude of the ocean-estuary exchange depends on the dynamics controlling the tidally averaged estuarine circulation. Therefore, the tidally averaged circulation is often referred to as the exchange flow. Exchange flow dynamics vary considerably from system to system and can be driven by buoyancy gradients (e.g., Hansen & Rattray, 1965; Lerczak et al., 2006) and tidal asymmetries (e.g., Burchard & Hetland, 2010; Jay & Musiak, 1996), and are modified by hydraulic control (Armi & Farmer, 1986; Stommel & Farmer, 1953), the Earth's rotation (e.g., Valle-Levinson, 2008), lateral curvature (e.g., Bo et al., 2023; Chant, 2002), local winds (e.g., Soto-

Riquelme et al., 2023), and non-local oceanic forcing related to upwelling winds and coastal stratification (Aure et al., 1996; Juarez et al., 2022; Klinck et al., 1981) among other mechanisms (see for reviews: Geyer & MacCready, 2014; MacCready & Geyer, 2010). The dynamics influencing a particular system will impact its sensitivity to stressors including climate change (Pareja-Roman & Chant, 2023). Therefore, understanding which forces contribute to observed hydrodynamic variability is essential for informed estuary management.

The Salish Sea is a large estuary on the Pacific Northwest coast that is an important hub of economic and ecological activity (Sobocinski et al., 2022). Both the Salish Sea and regional coastal ocean are threatened by increasing rates of harmful algal blooms, hypoxia, and acidification (Bianucci et al., 2018; Engel et al., 2025; Feely et al., 2008; Khangaonkar et al., 2018, 2019; Yamada et al., 2021). Ocean-estuary exchange plays a critical role as inflow from the coast can transport harmful algae and invasive larvae into the estuary (Brasseale et al., 2019; Giddings et al., 2014; Stone et al., 2022; Yamada et al., 2017) and estuary outflow can transport riverine materials to the coastal ocean (Mackas & Harrison, 1997; Wetz et al., 2006). Moreover, vertical mixing of inflowing oceanic water upward can lead to refluxing oceanic water (often high in nitrogen and lower in DO) back to the ocean with significant impact on coastal primary productivity (Cokelet & Stewart, 1985; Davis et al., 2014; MacCready et al., 2021). The Salish Sea is a deep (often >150 m) branching fjord system with intermittent sills and numerous rivers generating local regions of intense mixing alongside relatively quiescent basins (Broatch & MacCready, 2022). Investigations by MacCready and Geyer (2024) demonstrated that tidal pumping at constrictions and sills is the dominant mechanism driving exchange flow variability within parts of the Salish Sea interior, while Allen et al. (2025) find density-driven flow to also be important. Beyond local forces, the Salish Sea is subject to ocean forcing through offshore upwelling and downwelling winds (Giddings & MacCready, 2017; Thomson et al., 2007). These winds change the source of inflowing deep water (Alford & MacCready, 2014; Beutel & Allen, 2024; Brasseale & MacCready, 2025; Hickey et al., 2016; Stone et al., 2018) and periodically force relatively fresh Columbia River plume water into the strait (Masson, 2006). The effects of ocean forcing can be strong enough to reverse the exchange flow close to the mouth (Frisch et al., 1981; Giddings & MacCready, 2017; Holbrook & Halpern, 1982; Thomson et al., 2007). Many of the predicted impacts from climate change on the Salish Sea are related to changes in along-shelf wind-driven upwelling (Bograd et al., 2009; Foreman et al., 2011; Khangaonkar et al., 2019), but it is unclear how important upwelling effects are deep into the Salish Sea. The goal of this study is to delineate the roles of local (tides and river discharge) and remote (i.e., ocean) forcing on exchange flow dynamics. We seek to answer the questions: what are the limits of oceanic influence on the Salish Sea, and what does this say about the general role of oceanic forcing on estuarine exchange flow and tracer transport?

2. Background

The Salish Sea is composed of three main bodies: the Strait of Juan de Fuca, the Strait of Georgia and the Puget Sound (Figure 1a). The Strait of Juan de Fuca is the primary connection for the Salish Sea to the coastal ocean. Near the mouth of the Strait of Juan de Fuca the circulation is impacted by the seasonally varying offshore Juan de Fuca Eddy (Foreman et al., 2008), the initiation of the Vancouver Island Coastal Current (Hickey et al., 1991), and Columbia River plume intrusions (Holbrook & Halpern, 1982). The dynamics controlling flow within the Strait of Juan de Fuca itself are influenced by the earth's rotation and tidal rectification, but local differences in the Coriolis, advective, and pressure gradient forces largely compensate one another (Giddings & MacCready, 2017; Martin & MacCready, 2011). The resulting exchange flow, although locally influenced by rotation (e.g., Thomson et al., 2007), is proportional to the along-strait pressure gradient (Giddings & MacCready, 2017). The Strait of Juan de Fuca is separated from the Strait of Georgia to the north by Haro Strait and the waterways around the Gulf and San Juan Islands. Haro Strait is a deep channel bound by relatively shallow sills. Haro Strait is downstream of the Fraser River, the primary discharge into the Strait of Georgia, which peaks in late spring to early summer. The local circulation in the Haro Strait is hydraulically controlled with large fortnightly variability that sets the oceanic conditions for intermediate and deep inflow into the Strait of Georgia (Pawlowicz, 2002; Stevens et al., 2021; Thomson et al., 2020). A substantial amount of oceanic origin water that reaches Haro Strait is "refluxed" or mixed upwards toward the surface and flows back out of the Salish Sea without reaching the Strait of Georgia interior (Allen et al., 2025; Beutel & Allen, 2024; Cokelet & Stewart, 1985; MacCready et al., 2021; Masson, 2006); however, during the upwelling season dense water from the Strait of Juan de Fuca can drive renewal in the Strait of Georgia (Masoud & Pawlowicz, 2023; Pawlowicz et al., 2019). Although the circulation within Haro Strait is heavily modulated by tidal variability, Lagrangian particle analysis has shown that the net

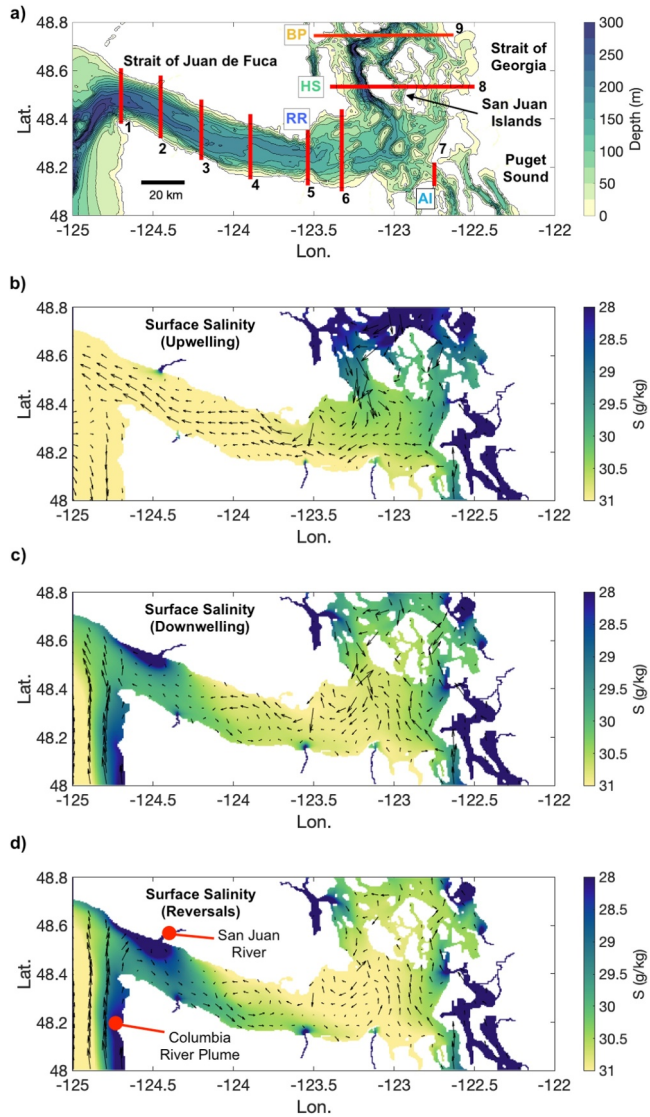

Figure 1. (a) Bathymetry of study region. Full model domain in Figure S1 in Supporting Information S1. The red lines are sections used for correlation analysis. The location of Race Rocks (RR), Admiralty Inlet (AI), Haro Strait (HS), and Boundary Pass (BP) are lines 5, 7, 8, and 9, respectively. (b) Surface salinity and current vectors averaged during upwelling time periods. (c) Same as (b) but during downwelling time periods. Note the direction of the offshore current is north. (d) Same as (c) but during reversing time periods. Plumes from two of several freshwater sources, the Columbia River (CR) and San Juan River, are indicated in red.

exchange between the Strait of Juan de Fuca and the Strait of Georgia is tied to density differences between the two basins (Allen et al., 2025). The Strait of Juan de Fuca also connects with Puget Sound through a narrow sill region, Admiralty Inlet, on its southeast corner. Similar to Haro Strait, spring-neap variability at Admiralty Inlet heavily influences the circulation and renewal of Puget Sound (Geyer & Cannon, 1982; MacCready & Geyer, 2024), with periodic upwelled dense water also initiating renewal (Cannon et al., 1990; Deppe et al., 2018).

Ocean forcing has long been recognized to be an important contributor to exchange flow variability in the Salish Sea (e.g., Frisch et al., 1981; Holbrook & Halpern, 1982), but the definition of ocean forcing can vary from study to study and more broadly from system to system. In this study, we define ocean forcing to refer to the variability in coastal water properties, stratification, and sea surface height which in this region is primarily associated with along-shelf upwelling and downwelling winds but is also influenced by coastal trapped waves and undercurrent

variability. During downwelling, this includes the effect of the coastal trapped Columbia River plume in addition to the traditional effects of raised sea surface height and depressed isopycnals (see Giddings and MacCready (2017)). Here, transient events refer to when downwelling-favorable winds force the Columbia River plume into the Strait of Juan de Fuca as a surface intrusion (Thomson et al., 2007). In other contexts, coastal intrusions can describe relatively dense water that is upwelled (e.g., Willapa Bay; Hickey et al., 2002) into estuaries, but we are primarily focused on buoyant intrusions from the Columbia River. Although the sources of oceanic variability might be different in other systems (e.g., storms on the U.S. east coast), they can be broadly considered as variability in coastal density, stratification, and sea surface height, and thus we hope the results will have parallels in other systems despite the unique geometry of the Salish Sea.

For analysis, we use the total exchange flow (TEF) method to evaluate the exchange flow variability spatially and temporally (Lemagie et al., 2022; Lorenz et al., 2019; MacCready, 2011; MacCready et al., 2018). Applying TEF to a cross-section returns subtidal bulk values for incoming/outgoing volume transport Q_{in}/Q_{out}, and incoming/outgoing transport-weighted salinities S_{in}/S_{out}. Using these bulk values and river discharge Q_R, an expression for the subtidal salt budget of a system can be constructed as follows:

$$\frac{d}{dt}\int S dV = Q_{in}\Delta S - Q_R S_{out}, \tag{1}$$

where the left hand side is volume integrated salt storage from the mouth to the head of the estuary, the second term is the exchange or import of salt at the mouth, and the final term is the freshwater flushing of salt (Broatch & MacCready, 2022; MacCready et al., 2021). TEF allows separate analysis of both Q_{in} and the salinity difference $\Delta S = S_{in} - S_{out}$ which together make up the landward transport of salt due to the exchange flow $Q_{in}\Delta S$ (MacCready & Geyer, 2024). Note, the outflowing water $Q_{out} = Q_{in} + Q_R$, but in the absence of freshwater and saltwater mixing, Q_{out} will simply be the river flow and Q_{in} will be 0. Therefore, Q_{in} is more appropriately tied to the strength of the exchange and we will use Q_{in} synonymously with exchange flow (MacCready, 2011). We will also refer to $Q_{in}\Delta S$ as the salt exchange. In steady state, the salt budget reduces to the Knudsen relation as follows (Burchard et al., 2018; Knudsen, 1900):

$$Q_{in} = Q_R \frac{S_{out}}{\Delta S}. \tag{2}$$

MacCready and Geyer (2024) worked through possible scalings for the salt exchange as a function of tidal velocity amplitude U_{tide} based on the theories of gravitational circulation and tidal pumping (see Text S1 in Supporting Information S1 for details and caveats). Briefly, in a tidal-pumping dominated regime, typically associated with strong tides and bathymetric changes (Garcia & Geyer, 2023), the exchange flow increases with tidal current.

$$Q_{in} \propto U_{tide}. \tag{3}$$

Note that because Equation 3 is proportional to, the units need not match as there are constant multipliers which have units (see Text S1 in Supporting Information S1 or MacCready and Geyer (2024)). While in a gravitational circulation regime there is a balance between the salinity gradient, dS/dx, and tidally driven vertical mixing, K, such that

$$Q_{in} \propto \frac{1}{K}\frac{dS}{dx}. \tag{4}$$

If we are only considering changes due to tidal current variability and we assume that the salinity gradient is slow to adjust to changes in tidal mixing and that vertical mixing K is proportional to tides, then

$$Q_{in} \propto \frac{1}{U_{tide}}, \tag{5}$$

and the exchange flow decreases with tidal current (Hansen & Rattray, 1965).

The stratification associated with gravitational circulation can be generated through straining or tilting of the background salinity gradient by the exchange flow and reduced through mixing (MacCready & Geyer, 2010). That is, the inflow transports saltier water into the estuary at depth while the outflow transports relatively fresh water at the surface increasing stratification in the middle. Using Equation 4, a scaling for stratification is given by the following equation:

$$\Delta S \propto \frac{Q_{\text{in}}}{K}\frac{\mathrm{d}S}{\mathrm{d}x} \propto \frac{1}{K^2}\left(\frac{\mathrm{d}S}{\mathrm{d}x}\right)^2, \tag{6}$$

which considering only tidal variability reduces to the scaling as follows:

$$\Delta S \propto \frac{1}{U_{\text{tide}}^2}. \tag{7}$$

Ultimately, MacCready and Geyer (2024) found that within the San Juan Islands and Puget Sound the exchange flow was largely consistent with tidal pumping and Equation 3 while stratification was consistent with Equation 7. We use these scalings as the expected response of the exchange flow to tidal amplitude and acknowledge that these observed relationships have two different explanatory theories.

We can generate predictive relationships for the exchange flow response to ocean forcing by utilizing the results of Giddings and MacCready (2017). They showed the exchange flow in the Strait of Juan de Fuca to be proportional to the along-strait pressure gradient which is proportional to along-shelf wind stress. This exchange flow response occurs because upwelling increases both the salinity (and therefore density) of water and lowers the sea-surface height at the ocean end of the estuary. This process increases baroclinic and barotropic pressure gradients, while the reverse occurs during downwelling favorable winds. Thus, similar to gravitational circulation (Equation 4)

$$Q_{\text{in}} \propto \frac{\partial P}{\partial x} \propto \frac{\partial S}{\partial x} \propto -W_{\text{maj}}. \tag{8}$$

where $\mathrm{d}P/\mathrm{d}x$ and $\mathrm{d}S/\mathrm{d}x$ are the along-strait pressure and salinity gradients and W_{maj} is an index representing the strength of the along-shelf wind stress (i.e., downwelling/upwelling favorable, discussed Section 3.2). The primary assumption in Equation 8 is that the offshore salinity is proportional to along-shelf wind stress and changes the ocean-estuary salinity gradient. Using Equation 6, if we assume that vertical stratification is created and maintained by exchange flow straining of horizontal salinity gradients and that the salinity gradient is proportional to wind stress then,

$$\Delta S \propto Q_{\text{in}}\frac{\partial S}{\partial x} \propto -W_{\text{maj}}|W_{\text{maj}}|, \tag{9}$$

where Q_{in} is always positive and comes from Equation 8. We use these scaling relationships as guides in interpreting the drivers of exchange flow variability within the strait.

3. Method

3.1. Model

Our study uses a 3D hydrodynamic simulation of the Salish Sea and nearby coastal ocean called LiveOcean (Figure 1a). The model is described in full detail, including validation against observations, in MacCready et al. (2021). LiveOcean has been used in numerous studies investigating both physical and biogeochemical processes (Brasseale & MacCready, 2025; Broatch & MacCready, 2022; Du et al., 2024; MacCready & Geyer, 2024; Stone et al., 2022; Xiong et al., 2024). The model was built using regional ocean modeling system (Shchepetkin & McWilliams, 2005), which includes 30 terrain-following sigma coordinate layers and has horizontal resolution varying from 500 m within the Salish Sea that stretches to 3 km at the coastal boundaries. The model uses realistic external forcing including open ocean boundary conditions of velocity, temperature, and salinity from a global data-assimilative model, 8 tidal constituents imposed at the boundaries, 45 river sources,

and atmospheric forcing from the weather research and forecast (WRF) model (MacCready et al., 2021). We note that river discharges are scaled to account for ungauged watershed areas as described in MacCready et al. (2021) and following Mohamedali et al. (2011); however, it is good to keep in mind that this introduces some uncertainty, particularly in regions with fewer gauges such as along the southern edge of Vancouver Island. We use the output from a 5-year hindcast from 2017 to 2022 with instantaneous snapshots saved every hour.

3.2. Analysis

The drivers of the salt exchange are identified by calculating correlations between forcing terms and the TEF bulk terms. The TEF bulk terms were calculated using 1,000 salinity bins, a Godin filter to produce subtidal data (Thomson & Emery, 2014), and the dividing salinities method (Lorenz et al., 2019; MacCready, 2011; MacCready et al., 2018). Although we feel TEF provides great insight into exchange flow variability, there are several caveats regarding our TEF analysis. First, the accuracy of TEF depends on the model's ability to recreate salinity and salinity gradients. MacCready et al. (2021) note that this version of LiveOcean has a modest salinity bias high (0.65 g/kg) with the largest salinity errors close to the surface. The model also has relatively weak salinity gradients compared to observations. However, both of these biases are smaller within the Strait of Juan de Fuca than in the Salish Sea interior. Second, TEF provides an integrated view that collapses multiple layers into bulk variables which might misrepresent the full 3-dimensional aspects of the flow. For example, during reversals the exchange flow is composed of three layers (Figure S3 in Supporting Information S1). S_{in} is composed of salt transport from both the surface and deep layer. If the deeper layer dominates S_{in}, then $S_{\text{in}} > S_{\text{out}}$ and the flow will not be identified as reversed despite potential surface inflow. In this study, we keep these limits in mind and acknowledge that the relationships between TEF variables and external drivers are unlikely to be linear because they condense higher-order dynamics.

The forcing terms evaluated include river discharge Q_{R}, tidal velocity amplitude U_{tide}, and remote wind stress W_{maj}. Q_{R} includes all river discharge upstream of the section of interest and was not found to be strongly correlated with any exchange flow variability except at the entrance to the Strait of Georgia (Table S1 in Supporting Information S1). This finding is consistent with other studies of the Salish Sea (Babson et al., 2006; MacCready et al., 2021; Sutherland et al., 2011) and likely arises from the long adjustment time of the Salish Sea to changes in river flow (MacCready & Geyer, 2010). For these reasons, Q_{R} is negligible in higher-frequency analysis. U_{tide} is the maximum tidal velocity over a 24 hr period and captures fortnightly variability. Remote wind stress is represented with an along-shelf wind index W_{maj} (Austin & Barth, 2002; Giddings et al., 2014). The along-shelf wind stress index is a weighted sum of wind stress given by the following equation:

$$W_{\text{maj},k}(t) = \frac{1}{k}\int_{t_0}^{t} \tau_{\text{maj}} \mathrm{e}^{(t'-t)/k} \mathrm{d}t', \tag{10}$$

where τ_{maj} is the along-shelf wind stress (computed as the major principal axis component), k the time decay scale of the weighting, t_0 is the start time and t is time. W_{maj} accounts for the timescale for upwelling to reach equilibrium ($k = 8$ days, see Austin and Barth (2002)) and is more predictive of exchange flow dynamics than instantaneous wind stress (Giddings & MacCready, 2017). W_{maj} is defined as positive during downwelling-favorable (i.e., northward) conditions. Local wind stress can be important in Puget Sound and the Strait of Georgia (Griffin & LeBlond, 1990; Sutherland et al., 2011) but plays a lesser role in the Strait of Juan de Fuca (Giddings & MacCready, 2017, Table S1 in Supporting Information S1). Thus, references to "winds" refer to remote along-shelf winds unless explicitly stated otherwise.

The correlations between the drivers and bulk terms were calculated at cross-sections (e.g., Figure S2 in Supporting Information S1) along the strait (Figure 1a). For the correlations, we have removed periods of reverse flow ($\Delta S < 0$ at the mouth, 13% of record with typical gaps of 4 days) to focus on "normal" conditions. The correlation analysis is conducted on two timeseries of each variable. One is the full 5 years subtidal record during positive exchange conditions (SP), calculated with a Godin filter (Thomson & Emery, 2014). The Godin filter is a sequence of boxcar filters of length 24, 24, and 25 hr which targets diurnal and higher frequencies (e.g., Harvey et al., 2023). The other is band-pass filtered between subtidal and 20 days (BP) to enable analysis of spring-neap and synoptic variability. It was generated by applying a 20-day 4th-order high-pass filter to the SP record. Both of these timeseries contain spring-neap and synoptic variability, but the BP record removes lower frequencies such

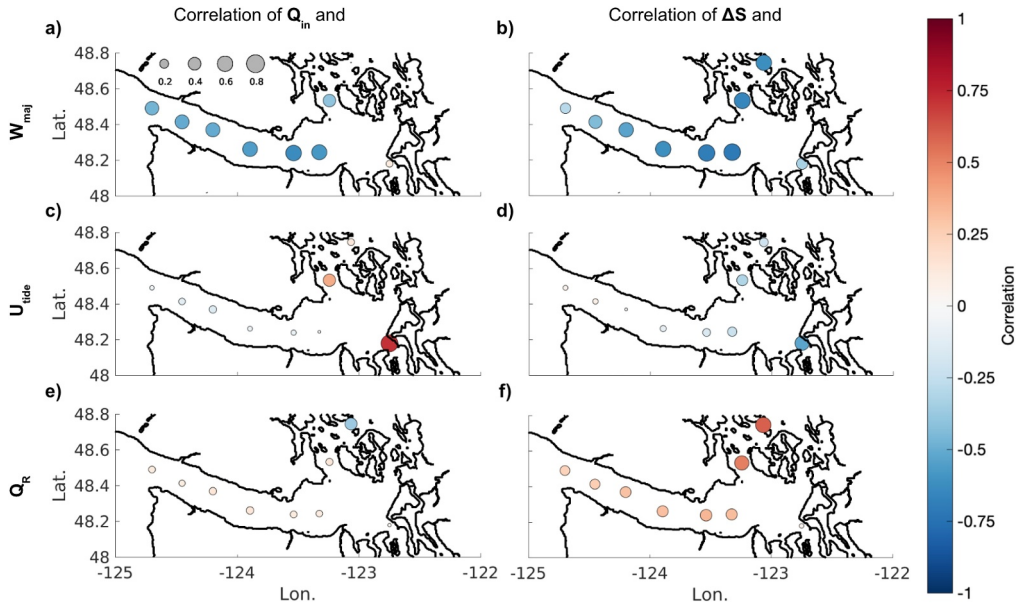

Figure 2. Correlation coefficient (r_S, circle size and color) between variables and forcing over the full subtidal positive exchange record (SP) at no lag. Recall that W_{maj} is negative during upwelling favorable winds such that a negative correlation between Q_{in} and W_{maj} implies that upwelling winds strengthens the exchange flow. (a) W_{maj} and Q_{in}, (b) W_{maj} and ΔS, (c) U_{tide} and Q_{in}, (d) U_{tide} and ΔS, (e) Q_R and Q_{in}, and (f) Q_R and ΔS.

as seasonal cycles. We use a Spearman correlation (r_S) which measures monotonic relationships whether the relationship is linear or not.

4. Results

4.1. Subtidal Positive (SP) Exchange Flow Variability

The exchange flow is expected to increase during upwelling conditions (Giddings & MacCready, 2017; Thomson et al., 2007). We find the subtidal inflowing volume transport is significantly correlated with upwelling winds along the whole Strait of Juan de Fuca (Figure 2a, Table S1 in Supporting Information S1) during positive exchange flow conditions. Recall that W_{maj} is defined to be negative for upwelling winds, so in this case the correlation coefficient varies from $r_S = -0.47$ to -0.61 along the strait. An example of the exchange flow variability is shown for the Race Rocks section (Figure 3a, dark blue). Here, the transport variability is dominated by the seasonal cycle and aligns with offshore wind conditions (Figure 3e) especially winter minima. However, weaker higher-frequency variability is also present (discussed in Section 4.2).

At the constrictions, the exchange flow variability becomes influenced by the tidal pumping mechanism. The tidal dominance is clearest within Admiralty Inlet separating Puget Sound and the Strait of Juan de Fuca (Figure 2c). There, the exchange flow variability (Figure 3a) is more correlated with tides ($r_S = 0.72$, Figure 2c) than with winds ($r_S = 0.12$, Figure 2a) or river discharge ($r_S = 0.03$, Figure 2e). Tidal impact on exchange flow variability is more balanced with remote winds at Haro Strait ($r_S = 0.39$ for tide vs. $r_S = -0.40$ for wind, Figures 2a and 2b) likely reflecting the greater depth in the strait, although the variance explained for either ($r_S^2 = 0.16$) is not particularly high. Outside of both constrictions, the importance of tidal pumping declines with along-channel distance (Figure 2b). Consequently, a picture of exchange flow dynamics in the western Salish Sea emerges. The exchange flow transport variability is controlled by remote wind stress in the Strait of Juan de Fuca until it is disrupted by local tidal pumping at narrow sill-influenced constriction zones within Admiralty Inlet and Haro Strait. The significance of tidal modulation of exchange flow strength varies between these locations but is consistent with MacCready and Geyer (2024) and Allen et al. (2025).

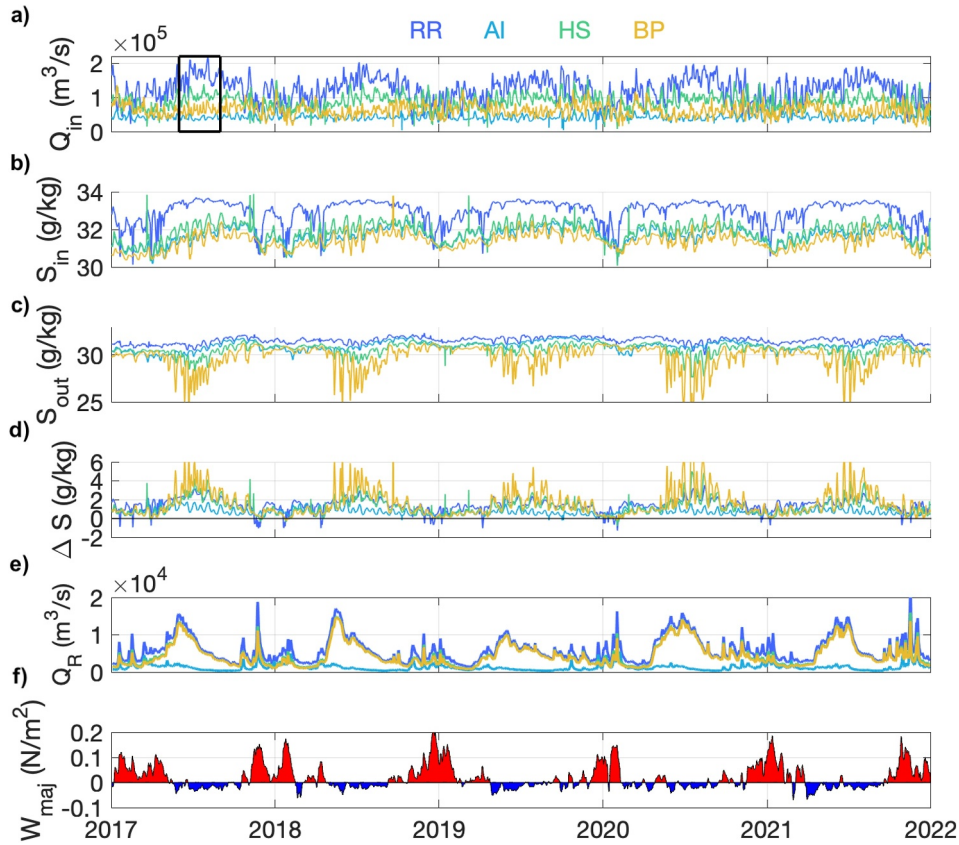

Figure 3. (a) Timeseries of Q_{in} at Race Rocks, Admiralty Inlet, Haro Strait, and Boundary Pass (Figure 1a, Line 5, 7, 8, and 9). (b) Same but for S_{in}. (c) Same but for S_{out}. (d) Same but for ΔS. Note that when $\Delta S < 0$ the exchange flow must be reverse. (e) River discharge upstream of sections. (f) Along-shelf wind strength where positive (red shading) is downwelling and negative (blue shading) is upwelling. The black box in panel (a) outlines the time period of Figure 4a.

4.2. Subtidal Positive Exchange Salinity Difference and Salt Exchange

Similar to the exchange flow, the stratification or salinity difference within the Strait of Juan de Fuca is correlated with upwelling winds (Figure 2b). This correlation corresponds physically with the upwelling of deeper isohalines into the system (Figure 4). Therefore, the correlation primarily arises through the relationship between remote wind stress and the S_{in} component of ΔS. Interestingly, the correlation magnitude of W_{maj} and ΔS appears to decrease substantially near the mouth of the strait, going from $r_S = -0.70$ near Race Rocks to $r_S = -0.27$ at the mouth. We attribute this pattern to the increasing influence of coastal stratification and hydrographic variability near the mouth, discussed more in Section 4.3. At Haro Strait, the correlation between upwelling and ΔS is high ($r_S = -0.65$, Figure 2b) compared to tidal pumping ($r_S = -0.19$, Figure 2d) which is surprising given the balance of the two terms in explaining exchange flow variability. Compare for example, the similarity of ΔS and Q_{in} at Race Rocks versus Haro Strait (Figure 3d). Additionally, there is relatively high correlation between Q_R and ΔS ($r_S = 0.53$). Moving past Haro Strait and into the Strait of Georgia through a section called Boundary Pass (Figure 1a, Line 9) these trends continue. Both remote wind stress and river discharge are correlated with ΔS ($r_S = -0.62$ for wind and $r_S = 0.61$ for discharge). Beyond Haro Strait, remote wind forcing and river discharge are technically significantly correlated with one another ($r_S = -0.32$, see Figure 3e) and so can confound analysis, but it is clear that the local buoyancy forcing is important to stratification. This is not the case at Admiralty Inlet, where ΔS is primarily explained by tidal pumping (Figure 2d, also MacCready and Geyer (2024)).

The net salt imported into the system depends on both the exchange flow and the salinity difference it acts upon. In a wind-dominated system, both ΔS and Q_{in} are enhanced by upwelling winds and an increase in net salt transport is reinforced. Consequently, the salt exchange, $Q_{\text{in}}\Delta S$, along the Strait of Juan de Fuca is correlated with upwelling winds (Figure 5a). Like ΔS, salt exchange correlation is weakest at the mouth and increases further into

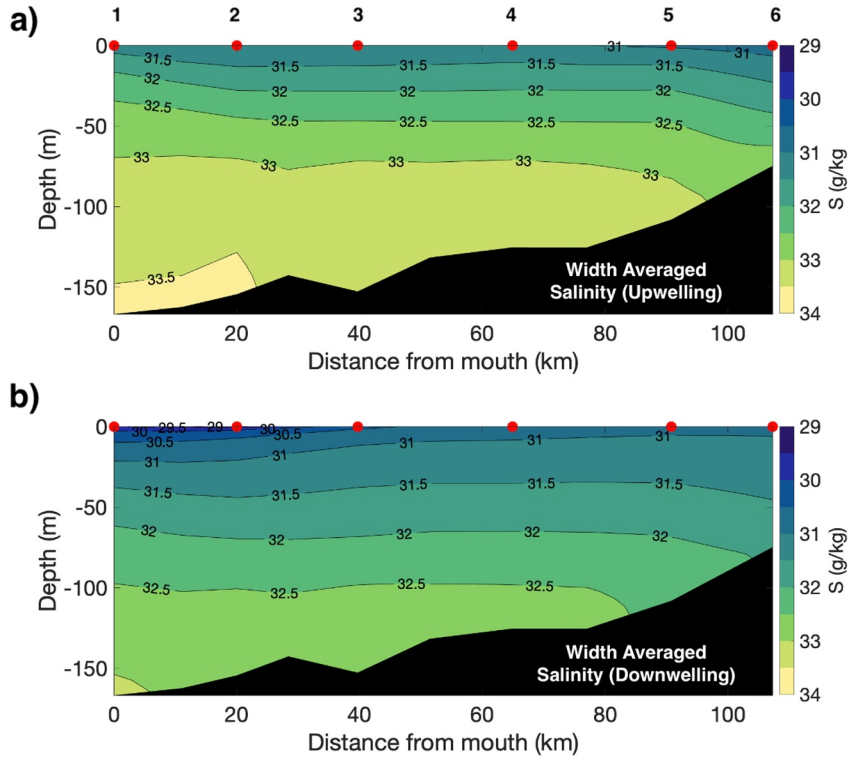

Figure 4. (a) Along-strait width-averaged salinity section during upwelling conditions. Red dots indicate the location of Sections 1–6 marked in Figure 1a. (b) Same as (a) but during all downwelling time periods (including during reversals).

the strait. Within Haro Strait and Boundary Pass, remote winds exert less influence on Q_{in}, but they still impact ΔS (Figure 2b). Since the variability in ΔS is greater than the variability in Q_{in}, the salt exchange variability is substantially correlated with coastal upwelling and downwelling (Figure 5). Although, we stress that it is difficult to distinguish between the effects of remote winds and river discharge closer to the Strait of Georgia. At the tidally dominated Admiralty Inlet, there is a tension between Q_{in} which increases with tidal velocities (Figure 2c) and ΔS which decreases with tidal mixing (Figure 2d). As a result, tides are weakly correlated with salt exchange ($r_S = 0.3$, Figure 5b). This correlation is only marginally higher than the correlation with along-shelf winds ($r_S = 0.28$). To summarize, the salt exchange in the Strait of Juan de Fuca is responsive to the seasonal cycle of along-shelf wind stress, and within Haro Strait and Boundary Pass is sensitive to both winds and river discharge, but the salt exchange does not have a clear signal at Admiralty Inlet.

4.3. Coastal Influence on Near-Mouth Variability

The region close to the mouth of the Strait of Juan de Fuca experiences increased variability of stratification, salinity, and circulation due to coastal influences. Freshwater from the Columbia River (CR) plume impinges on the coast during downwelling conditions and intermittently enters the mouth of the Salish Sea as a surface intrusion (Giddings & MacCready, 2017; Thomson et al., 2007). During periods of mouth flow reversals, the relatively fresh CR plume intrusions are easily visible alongside local contributions like the San Juan River (Figure 1d). During downwelling conditions more generally, the region that is close to the mouth is fresher than the mid-strait region (Figure 1c) despite weak surface flow. Mixing of the nearby river plumes (Broatch & MacCready, 2022) and CR plume water during previous intrusions (Masson, 2006) results in a low-salinity signal that persists even during normal conditions and likely contributes to the formation of the Vancouver Island Coastal Current (Hickey et al., 1991). The signal highlights a region of transient oceanic influence where both advection of coastal surface waters into the strait and retention of freshwater from the Strait of Juan de Fuca rivers leads to modification of near-mouth water properties including stratification. In addition, this region contains synoptic variability in density due to coastal trapped waves and the California Undercurrent which is not accounted for with W_{maj} (Thomson & Krassovski, 2015). The presence of these numerous coastal factors helps

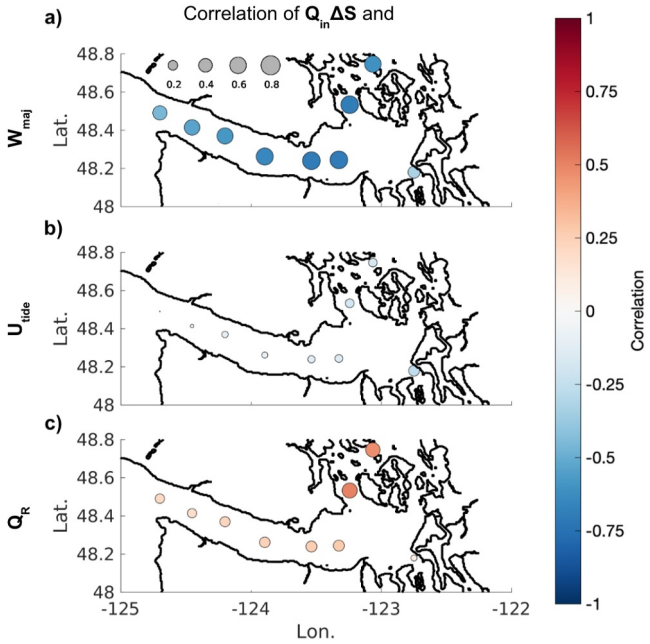

Figure 5. Correlation coefficient (circle size and color) between variables over the full subtidal positive exchange record (SP) at no lag. Recall that W_{maj} is negative during upwelling favorable winds. Scale for the circles is in panel (a). (a) W_{maj} and $Q_{in}\Delta S$, (b) U_{tide} and $Q_{in}\Delta S$, and (c) Q_R and $Q_{in}\Delta S$.

explain a counter-intuitive spatial pattern where the stratification correlation with coastal wind stress *increases* away from the coast. The unorthodox relationship between remote wind stress and coastal stratification variability is clearest when looking at section-averaged along-strait plots of salinity. The surface stratification is enhanced close to the mouth during the downwelling season (Figure 4b) but we expect stratification to be enhanced during the upwelling season through the upwelling of dense water (Figure 4a). For the reasons outlined in this section, the salt exchange variance relative to mean conditions is greatest at the mouth (Figure S4 in Supporting Information S1) and the wind stress correlation is weakest.

4.4. Salt Exchange Variability of Band-Pass Record

Although the salt exchange variability is dominated by the seasonal cycle, remote forcing also impacts the salt exchange on synoptic timescales. We use a band-pass filter between subtidal and 20 days to remove the seasonal cycle and focus on both spring-neap and synoptic variability. While the spring-neap variability is associated with a specific period (14.76 days), the synoptic variability associated with the wind is much more broadband (Figure S5 in Supporting Information S1). Transport variability at Admiralty Inlet and Haro Strait is correlated with the spring-neap variability, but other higher-frequency variability dominates at locations away from the constrictions (Figure 6). The cross-correlation between band-pass Q_{in} and W_{maj} is relatively high ($r_S = -0.5$) throughout the Strait of Juan de Fuca (Figure 7a). Note, the correlation is only statistically significant after taking into account a lag between wind forcing and velocity response. The lag of maximum correlation increases along the strait and is akin to a wave speed of 0.6–0.75 m/s. This speed is close to the estimated wave speed $c = 0.8$ m/s of a propagating internal Kelvin wave (Text S2 in Supporting Information S1). The magnitude of the high-frequency exchange flow variability is also consistent with the magnitude derived from an analytical model of an internal Kelvin wave (Text S2 in Supporting Information S1, Jackson et al., 2018; Sanchez et al., 2024). Therefore, in line with previous work (Giddings & MacCready, 2017; Holbrook & Halpern, 1982), we find Kelvin waves are a likely mechanism through which remote wind forcing is communicated to the strait and that the waves likely modulate the exchange flow. Stratification within the Strait of Juan de Fuca (Figure 7c) has a weaker correlation with wind stress than on seasonal timescales although it also exhibits an increasing trend in lag from the mouth.

On short, synoptic timescales (subtidal to 20 days), the stratification and volume transport in the strait interior appear more sensitive to local forcing and tidal velocity strength than on seasonal timescales. The spring-neap effects on stratification are evident at Admiralty Inlet as well as at Victoria Sill (L6) and Haro Strait (Figure 7d). Stratification at the latter two locations are primarily impacted by along-shelf wind stress over seasonal timescales but the band-pass filter helps emphasize the relationship with tidal forcing on fortnightly timescales. Physically, the longer timescale ΔS behavior is due to secular changes in inflowing salinity, while the fortnightly behavior is driven by changes in local mixing. We also note a significant correlation between W_{maj} and ΔS at Haro Strait, but this has a short lag.

5. Discussion

5.1. Identifying the Limits of Oceanic Forcing

We have identified remote along-shelf winds as the primary driver of the exchange flow within the Strait of Juan de Fuca until flow reaches Admiralty Inlet and the Haro Strait region. Beyond these two regions, salt exchange variability transitions to local control although where this transition occurs is difficult to identify in Haro Strait using correlation analysis. We examine the drivers of ΔS to better diagnose the relative strength of local versus oceanic forcing. ΔS variability arises due to changes in either the inflowing salinity, outflowing salinity, or mixing of the two. Upwelling and downwelling winds change the source of inflowing waters and primarily drive variability in S_{in} (Beutel & Allen, 2024; Brasseale & MacCready, 2025; Giddings et al., 2014; Hickey

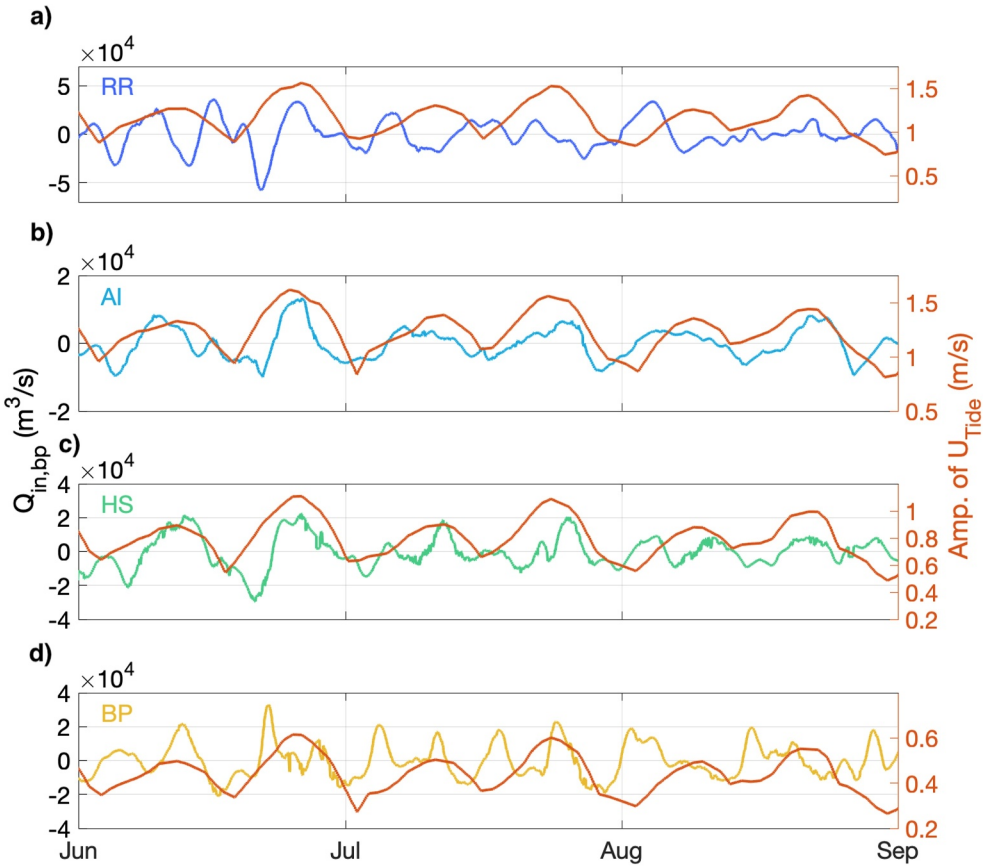

Figure 6. Timeseries of bandpass filter transport Q_{in} and tidal velocity U_{tide} over a 3 months window (Figure 3a) at (a) Race Rocks (RR), (b) Admiralty Inlet (AI), (c) Haro Strait (HS), and (d) Boundary Pass (BP). Note the scale of the y axis changes and that both variables are site specific.

et al., 2016). In contrast, the outflowing salinity S_{out} is primarily set by river discharge and mixing (Broatch & MacCready, 2022; MacCready & Geyer, 2024; MacCready et al., 2021). Since $\Delta S = S_{in} - S_{out}$, the variance in S_{in} relative to the variance in S_{out} gives a proxy for the relative importance of oceanic versus local (i.e., riverine, tidal) forcing in determining ΔS variability. We define the ratio

$$R_{\Delta S} = \frac{\sigma^2_{S_{in}} - \sigma^2_{S_{out}}}{\sigma^2_{S_{in}} + \sigma^2_{S_{out}}}, \tag{11}$$

to measure the importance of oceanic variability with the bottom term representing average variance. This ratio can range from -1 to 1 and when $R_{\Delta S} < 0$, $\sigma^2_{S_{out}}$ (i.e., local riverine/tidal mixing) dominates; when $R_{\Delta S} > 0$, $\sigma^2_{S_{in}}$ (i.e., remote ocean forcing) dominates; and when $R_{\Delta S} = 0$ both contribute equally. This ratio is >0 throughout much of the Strait of Juan de Fuca indicating remote forcing dominance there. The ratio goes from 0.35 at Race Rocks to -0.15 at Haro Strait (Figure 8a) to -0.75 at Boundary Pass. This indicates a transition from remote control of S_{in} within the Strait of Juan de Fuca to a balance between local buoyancy and remote forcing within Haro Strait to nearly complete local control by Boundary Pass. Closer to the mouth of the Strait of Juan de Fuca, the ratio is -0.125 indicating S_{out} variability is slightly stronger there too. This result is unsurprising given the observed influence of remnant freshwater from CR plume intrusions (Figures 1c and 1d). Importantly, in locations where ΔS is primarily driven by tidal mixing, such as Admiralty Inlet, the ratio will be closer to 0 even though local control is strong. At these locations, strong tidal mixing generates a high correlation between S_{in} and S_{out} (Figure 8b). This simple ratio alongside an assessment of mixing can work as a test in other estuaries to identify the source of salinity (and stratification) variability.

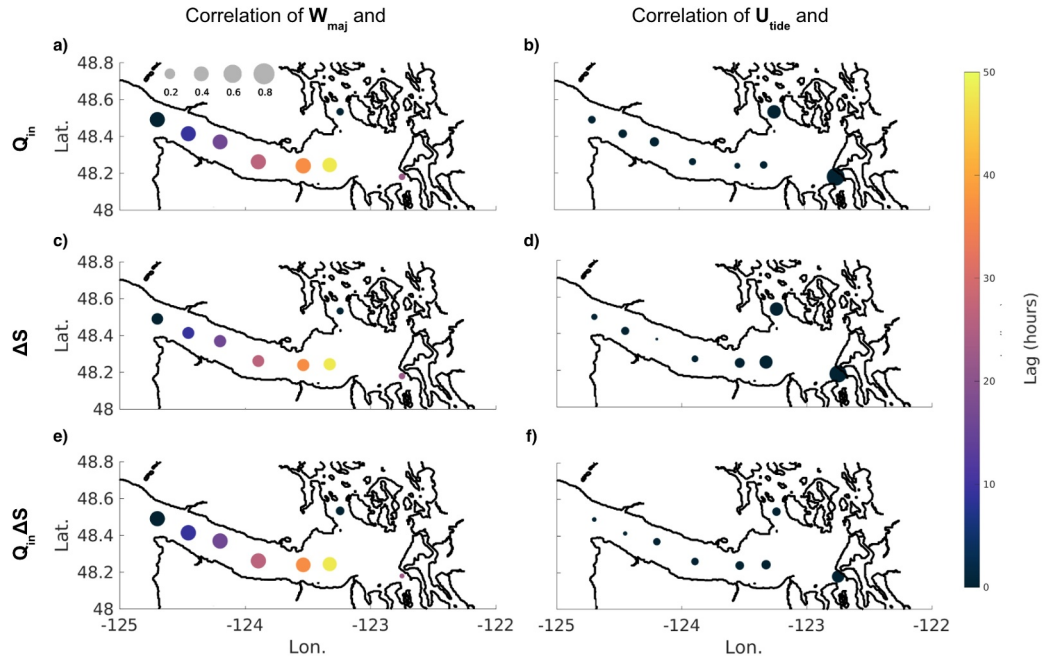

Figure 7. Correlation coefficient (circle size) between variables over the full band-pass record (BP) with lag (color) of maximum correlation. Recall that W_{maj} is negative during upwelling favorable winds. Scale for the circles is in panel (a). (a) W_{maj} and Q_{in}, (b) U_{tide} and Q_{in}, (c) W_{maj} and ΔS, (d) U_{tide} and ΔS, (e) W_{maj} and $Q_{in}\Delta S$, and (f) U_{tide} and $Q_{in}\Delta S$.

Another measure of the strength of local forcing is the freshwater Froude number (Fr_f) and mixing number (M) parameter space defined by Geyer and MacCready (2014). The freshwater Froude number $\mathrm{Fr}_f = \frac{U_r}{c}$ defined as the river velocity U_r over the internal wave speed c is a measure of local buoyancy forcing. The mixing number $M^2 = \left(\mathrm{C}_d U_{\mathrm{tide}}^2\right)/\left(\omega N_0 H^2\right)$ where C_d is the drag coefficient, ω is the tidal frequency, N_0 is stratification, and H is the water column depth is a measure of the local strength of tidal mixing. Within the Strait of Juan de Fuca, Fr_f is 10^{-4} to 10^{-3} indicating relatively weak freshwater forcing; for reference, an estuary with a higher river velocity such as the Columbia River has a Fr_f between 10^{-2} and 10^{-1}. Additionally, the mixing number M within the strait is small, 0.05, indicating relatively weak tidal mixing. Moving away from the mouth and further into the strait decreases the cross-sectional area, increasing both Fr_f and M (Figure S6 in Supporting Information S1). M increases to 0.12 at Race Rocks, but it is not until Admiralty Inlet ($M = 0.25$) that tidal amplitudes become strong enough to overwhelm oceanic variability. However, Fr_f remains low throughout the system consistent with weak river influence on exchange flow transport Q_{in}. Based on this classification system, we expect systems with weak local buoyancy or friction, that is, lying to the left and/or bottom of the Fr_f-M diagram, to be most sensitive to oceanic forcing. This includes deep estuaries such as fjords but also possibly low-inflow estuaries (Largier, 2023) and "tropical fjords" which despite not having great depth (or glacial origin), experience weak local forcing and are subject to renewal issues such as hypoxia (e.g., Adelson et al., 2022; Salamena et al., 2021).

5.2. Differences Between Haro Strait and Admiralty Inlet

Although we have grouped them together as "constrictions," Haro Strait and Admiralty Inlet behave quite differently and provide an example of how oceanic forcing transitions to local forcing in a region impacted by river forcing and tides respectively. Admiralty Inlet, which is shallow and narrow, is tidally dominated (MacCready & Geyer, 2024) and the spring-neap cycle controls variability in salt exchange on both short (<20 days) and longer time periods with occasional upwelling induced refreshment (Deppe et al., 2018). The transition from remote forcing to local forcing is immediate, as evident in the correlation analysis (Figure 2). The region around Haro Strait and into Boundary Pass is deeper and connects to a large freshwater source from the Fraser River. Although, this region has sills and also experiences fortnightly modulation in exchange flow (Thomson et al., 2020), it has weaker local control of ΔS over seasonal timescales (Figure 3). The flow through

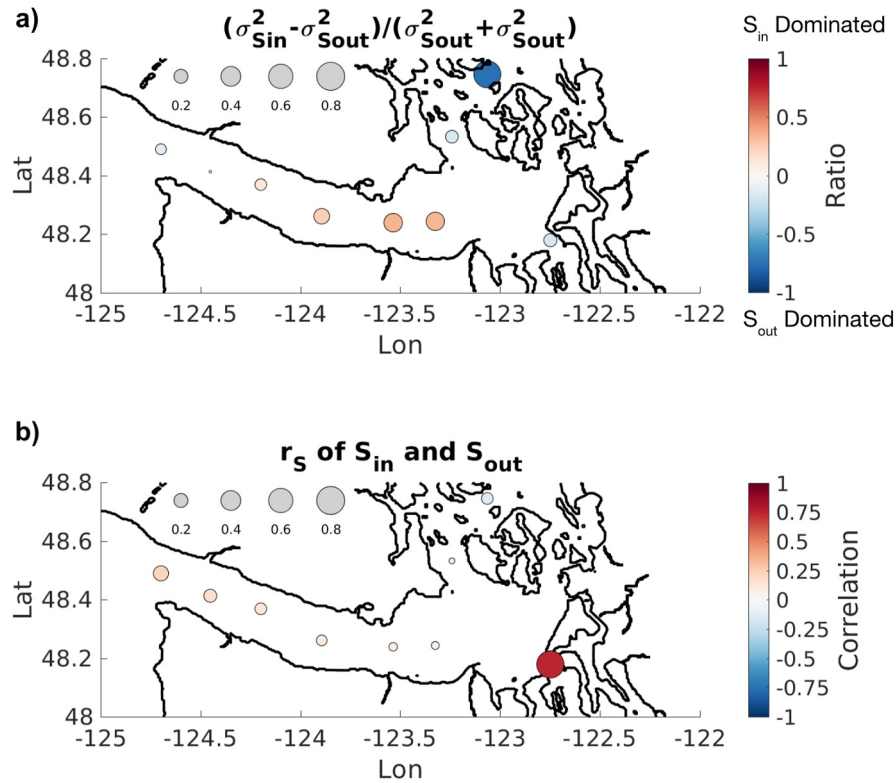

Figure 8. (a) Map of the Strait of Juan de Fuca with circles indicating the relative strength of S_{in} variance to S_{out} variance. A smaller circle indicates a more balanced variance of S_{in} and S_{out}. The color indicates whether the variance of S_{in} (red) or S_{out} (blue) is higher. (b) Similar to Figure 2, circle size and color indicates the correlation between S_{in} and S_{out}. When correlation is high, local mixing is presumably also high.

connecting the Strait of Juan de Fuca and the Strait of Georgia is primarily density driven, with tidal mixing reducing exchange (Allen et al., 2025). Consequently, the transition from remote to local control of salt transport is less abrupt. Since remote forcing and discharge share similar seasonal cycles, it is also difficult to distinguish the effects of upwelling from river flow on stratification. The forcing effects are instead best viewed through the lens of inflowing salinity and outflowing salinity. While significant mixing complicates this interpretation, significant mixing is also a sign of local control. Interestingly, both Haro Strait and Admiralty Inlet are tidally impacted on short timescales (Figure 7) and so the differences only arise over seasonal timescales.

5.3. Transient and Low-Frequency Oceanic Forcing

The spatial trends in salt exchange correlation imply multiple length scales through which oceanic forcing impacts salt exchange. Specifically, we identify a region close to the mouth which is sensitive to transient oceanic forcing and a region further into the strait which more effectively responds to low-frequency forcing from alongshelf winds. The transient forcing modifies the estuary water through advection of coastal water into the strait, often at the surface (Figure 1d), and is associated with increased synoptic variability and an interior salinity maxima sometimes referred to as a salt plug (Juarez et al., 2020, 2022). Even though flow reversals were removed from the correlation analysis, vertical mixing during these events helped maintain the relatively fresh signal from transient ocean forcing.

Further into the Strait of Juan de Fuca, the effects of higher-frequency variability are reduced, and the exchange flow responds primarily to remote forcing indirectly through adjustment to along-strait pressure gradients (Giddings & MacCready, 2017; Martin & MacCready, 2011). Recall that although the exchange flow is mostly geostrophic, the across-strait pressure gradients are proportional to the along-strait pressure gradients. In this region of lower-variance low-frequency forcing, exchange follows the seasonal offshore wind patterns. The ocean forcing is then primarily being communicated to the exchange flow as an additional slowly varying boundary condition.

Given their different dynamical responses to remote forcing, it is worth considering what sets the length scales separating transient from low-frequency oceanic influence. Physically, this might be thought of as the distance an oceanic intrusion travels during a remote wind event. Possible dynamic intrusion length scales include a diffusive length scale (Hickey et al., 2002) or an advective shelf intrusion length scale (Jackson et al., 2018). The diffusive length scale $L_{diff} = \sqrt{K_H T_{force}}$ where K_H is a horizontal diffusivity and T_{force} is the forcing period is appropriate for a tidally driven residual flow, such as nearby Willapa Bay (Banas et al., 2004; Hickey et al., 2002), but is unlikely to describe the Strait of Juan de Fuca. Instead, an advective shelf intrusion length scale $L_{in} = U_{in} T_{force}$ where U_{in} is the inflowing velocity at the mouth seems more appropriate and has been applied to glacial fjords (Jackson et al., 2018). In the case of a glacial fjord and the Strait of Juan de Fuca, the increase in advection might be physically linked with a propagating Kelvin wave. If we set $T_{force} = 8$ days as the forcing timescale of the system (note this timescale is close to the decorrelation timescale of Q_{in} of 8.3 days), then T_{force} and the TEF calculated U_{in} produce a length scale of about 50 km during normal conditions and 55 km during flow reversals.

We can also consider a length scale set by bathymetry and strait geometry. The average front position separating relatively fresh and relatively salty water at the surface (Figure 1d) coincides with a shoaling and shifting of the strait thalweg, channel expansion and a surface recirculation cell (near Line 4, Figure 1a) around 60 km into the strait. The recirculation has been described in Martin and MacCready (2011) as the Port Angeles Depression Dome (PADD), a region of relatively low sea surface height found in the lee of Victoria Sill near Race Rocks. We find that only 33% of reversal events, associated with the strongest wind forcing, can extend beyond Race Rocks into the Salish Sea interior. In comparison, a coarser version of this model which did not exhibit the PADD had over 90% of reversal events reach into the Salish Sea interior (Table S2 and Figure S7 in Supporting Information S1). The bathymetric length scale is close to that estimated from the advective length scale approach. While it is possibly coincidental, one can imagine a scenario where the flow in the western part of the Strait of Juan de Fuca adjusts to local features such that the advective length scale is set by changes in bathymetry and geometry. Ultimately, we do not test the bathymetric control hypothesis and leave it to future work.

The region sensitive to transient forcing is the part of the Salish Sea most likely to be affected by the coastal transport of surface-trapped larvae or harmful algal blooms (Brasseale et al., 2019; Giddings et al., 2014; Yamada et al., 2021). Intrusions in late fall, when the ocean is still warm, are especially critical times for the landward transport of invasive Green crabs into the Salish Sea (Yamada et al., 2017). In this simulation, we find that only the largest downwelling events are able to produce reversals in salt exchange which extend deep inside the Salish Sea interior. The majority of the reversals (2/3) do not reach past Victoria Sill and Race Racks. However, a reversal is defined by a change in sign in ΔS related to TEF. When the flow is multi-layered, it is possible for the surface to be inflowing but for the total ΔS to remain positive (see Section 3.2). For example, at Race Rocks, the salt exchange is reversed only 4% of the time, but the net surface transport is inflowing 17% of the time. Therefore, even though full reversals of estuarine exchange are limited, there frequently exists a pathway for shelf tracers to be advected into the Salish Sea at the surface, consistent with previous studies of larval dispersal (Brasseale et al., 2019; Engel et al., 2025; Yamada et al., 2017). Given the differences between this model and previous models of the Salish Sea (Giddings & MacCready, 2017) in the number of reversals, it is worth investigating the sensitivity of the reversals to river discharge distribution along the northern edge of the Strait of Juan de Fuca, tides, horizontal recirculation, and model resolution in the future. It is also worth considering multi-layer TEF (Lorenz et al., 2019), Lagrangian particle tracking (Allen et al., 2025; Beutel & Allen, 2024), and/or numerical dye tracers (Giddings & MacCready, 2017) when looking carefully at transport pathways.

5.4. Connection to Biogeochemistry and Climate Change

The role of ocean forcing can also be understood in the context of biogeochemical variables influenced by upwelling such as nitrogen. The largest source and sink of nitrogen in the Salish Sea is the open boundary with the ocean (Mackas & Harrison, 1997; Sutton et al., 2013). Moreover, the efficient upward mixing of this ocean-derived nitrogen into the upper water column and export via the estuarine exchange flow plays a critical role in delivering deep nitrogen to the near-surface coastal ocean and contributes to the overall high coastal productivity in this region (Davis et al., 2014). Therefore, it is important to identify whether variability in nitrogen exchange is due to variability in the exchange flow or variability in oceanic nitrogen, both of which can increase during upwelling (Khangaonkar et al., 2019). Recent work by Xiong et al. (2024) answers this question with a

heat, total nitrogen and dissolved oxygen budget of the Salish Sea. The total nitrogen and the exchange flow variability within the Strait of Juan de Fuca are coupled (similar to our salt exchange), but the authors use averages to separate out the relative contributions of each term to the total nitrogen exchange ($Q_{in}\Delta N$ in exchange notation). The authors find that it is the variability in inflowing and outflowing total nitrogen (ΔN) rather than exchange flow variability (Q_{in}) which controls the magnitude of nitrogen exchange. Although biogeochemical variables are not conserved in the same manner as salinity (e.g., they are more sensitive to surface fluxes), we can imagine how our results might apply to that study. Since the nitrogen variability is tied to upwelling, we hypothesize that the remote wind-driven tracer signal observed within the Strait of Juan de Fuca persists into the Strait of Georgia. At Admiralty Inlet, ΔS and, presumably, ΔN become controlled by local tidal mixing. The implications for Puget Sound are that while incoming nitrogen fluxes are impacted by upwelling, the variability in nitrogen exchange will likely be dominated by fortnightly variability. In addition to biogeochemical impacts, we briefly comment on how these results might apply under climate change. Upwelling patterns are projected to intensify in the future (Foreman et al., 2011; Rykaczewski et al., 2015), although there exists significant uncertainty in the strength of changes (Bograd et al., 2023; Rykaczewski et al., 2015). Since ocean forcing dominates salt variability within the Strait of Juan de Fuca and up into Haro Strait, we can assume that this region could experience increased salt exchange resulting in an increase in salt content and connectivity with the shelf. The sensitivity of the exchange flow to oceanic forcing and the impact on biogeochemical parameters and response to climate change remain important areas for future research.

6. Conclusions

Our study shows that the limit of oceanic influence on the Salish Sea exchange flow depends on the time scales of interest (spring-neap or seasonal), the type of oceanic influence (low-frequency boundary variability or transient surface intrusions) and the dominant mode of local forcing (tides or river discharge). Generally, oceanic forcing related to upwelling and downwelling appears to drive variability of the volume and salt exchange all throughout the Strait of Juan de Fuca until it is disrupted at the narrow constrictions and sills: Haro Strait and Admiralty Inlet. While not entirely unexpected, the results suggest that the ocean forcing signal persists beyond earlier constrictions and sills (e.g., Race Rocks) and that Haro Strait and Admiralty Inlet behave differently in response to ocean forcing. Specifically, over seasonal timescales the ocean-driven variability in ΔS modifies the salt exchange deep into Haro Strait before transitioning into a local river influenced ΔS. At Admiralty Inlet, which is known for strong tidal pumping, the ocean forcing signal is immediately disrupted and the salt exchange becomes tidally dominated.

Counter-intuitively, the response to oceanic forcing right near the system mouth is less coherent and does not follow the overall trend of ocean forcing decreasing as one moves into the estuary. This region experiences increased variability in exchange and stratification due to the presence of direct wind forcing, surface intrusions of the Columbia River Plume, and local freshwater sources. Therefore, our results highlight that the impacts of ocean forcing manifest in different ways across different regions of the Salish Sea. Close to the mouth, fjord properties are sensitive to transient ocean forcing including buoyant surface intrusions. Further inside, fjord exchange treats offshore variability as a boundary condition on along-fjord salinity and pressure gradients.

Future research directions will be to analyze other upwelling sensitive systems, for example, Pacific Northwest estuaries Willapa Bay and Coos Estuary. Studying estuaries that are shallower than the Salish Sea and have their own unique geometry will help to broaden the application of these findings. Moreover, we hope that the ocean influence ratio parameter that we present (Equation 11) will be applicable to look at the relative importance of oceanic to local forcing in a variety of systems.

Data Availability Statement

The LiveOcean model has been previously published. Extractions for the Live Ocean model for 2017–2019 are available from MacCready (2023) using zenodo link: https://zenodo.org/doi/10.5281/zenodo.10206344.

The model extractions used in this paper are available at Sanchez (2025) using the link: https://zenodo.org/doi/10.5281/zenodo.13119092.

The model extractions contain hourly fields of u, v, temp, and salt.

Acknowledgments
We acknowledge Parker MacCready for generous access to the Live Ocean model and many insightful conversations as well as valuable feedback from two anonymous reviewers. This material is based upon work supported by the National Science Foundation under Giddings' NSF CAREER Award 1944735. Any opinions, findings, and conclusions or recommendations expressed in this material are those of the authors and do not necessarily reflect the views of the National Science Foundation.

References

Adelson, A. E., Altieri, A. H., Boza, X., Collin, R., Davis, K. A., Gaul, A., et al. (2022). Seasonal hypoxia and temperature inversions in a tropical bay. *Limnology & Oceanography*, *67*(10), 2174–2189. https://doi.org/10.1002/lno.12196

Alford, M. H., & MacCready, P. (2014). Flow and mixing in Juan de Fuca Canyon, Washington. *Geophysical Research Letters*, *41*(5), 1608–1615. https://doi.org/10.1002/2013GL058967

Allen, S. E., Soontiens, N. K., Dunphy, M., Olson, E. M., & Latornell, D. J. (2025). Controls on exchange through a tidal mixing hotspot at an estuary constriction. *Journal of Physical Oceanography*, *55*(4), 415–433. https://doi.org/10.1175/JPO-D-24-0001.1

Armi, L., & Farmer, D. M. (1986). Maximal two-layer exchange through a contraction with barotropic net flow. *Journal of Fluid Mechanics*, *164*, 27–51. https://doi.org/10.1017/S0022112086002458

Aure, J., Molvær, J., & Stigebrandt, A. (1996). Observations of inshore water exchange forced by a fluctuating offshore density field. *Marine Pollution Bulletin*, *33*(1), 112–119. https://doi.org/10.1016/S0025-326X(97)00005-2

Austin, J. A., & Barth, J. A. (2002). Variation in the position of the upwelling front on the Oregon shelf. *Journal of Geophysical Research*, *107*(C11), 1-1–1-15. https://doi.org/10.1029/2001JC000858

Babson, A. L., Kawase, M., & MacCready, P. (2006). Seasonal and interannual variability in the circulation of Puget Sound, Washington: A box model study. *Atmosphere-Ocean*, *44*(1), 29–45. https://doi.org/10.3137/ao.440103

Banas, N. S., Hickey, B. M., MacCready, P., & Newton, J. A. (2004). Dynamics of Willapa Bay, Washington: A highly unsteady, partially mixed estuary. *Journal of Physical Oceanography*, *34*(11), 2413–2427. https://doi.org/10.1175/JPO2637.1

Banas, N. S., MacCready, P., & Hickey, B. M. (2009). The Columbia River plume as cross-shelf exporter and along-coast barrier. *Continental Shelf Research*, *29*(1), 292–301. https://doi.org/10.1016/j.csr.2008.03.011

Bao, W., & Moffat, C. (2024). Impact of shallow sills on circulation regimes and submarine melting in glacial fjords. *The Cryosphere*, *18*(1), 187–203. https://doi.org/10.5194/tc-18-187-2024

Beutel, B., & Allen, S. E. (2024). Seasonal and interannual Salish Sea inflow origins using Lagrangian tracking. *Journal of Geophysical Research: Oceans*, *129*(6), e2023JC020106. https://doi.org/10.1029/2023JC020106

Bianucci, L., Long, W., Khangaonkar, T., Pelletier, G., Ahmed, A., Mohamedali, T., et al. (2018). Sensitivity of the regional ocean acidification and carbonate system in Puget Sound to ocean and freshwater inputs. *Elementa: Science of the Anthropocene*, *6*, 22. https://doi.org/10.1525/elementa.151

Bo, T., Ralston, D. K., & Geyer, W. R. (2023). Sources of drag in estuarine meanders: Momentum redistribution, bottom stress enhancement, and bend-scale form drag. *Journal of Physical Oceanography*, *53*(7), 1629–1650. https://doi.org/10.1175/JPO-D-22-0211.1

Bograd, S. J., Jacox, M. G., Hazen, E. L., Lovecchio, E., Montes, I., Buil, M. P., et al. (2023). Climate change impacts on eastern boundary upwelling systems. *Annual Review of Marine Science*, *15*(1), 303–328. https://doi.org/10.1146/annurev-marine-032122-021945

Bograd, S. J., Schroeder, I., Sarkar, N., Qiu, X., Sydeman, W. J., & Schwing, F. B. (2009). Phenology of coastal upwelling in the California Current. *Geophysical Research Letters*, *36*(1), L01602. https://doi.org/10.1029/2008GL035933

Boyer, E. W., Goodale, C. L., Jaworski, N. A., & Howarth, R. W. (2002). Anthropogenic nitrogen sources and relationships to riverine nitrogen export in the northeastern U.S.A. *Biogeochemistry*, *57*(1), 137–169. https://doi.org/10.1023/A:1015709302073

Brasseale, E., Grason, E. W., McDonald, P. S., Adams, J., & MacCready, P. (2019). Larval transport modeling support for identifying population sources of European Green Crab in the Salish Sea. *Estuaries and Coasts*, *42*(6), 1586–1599. https://doi.org/10.1007/s12237-019-00586-2

Brasseale, E., & MacCready, P. (2025). Seasonal wind stress direction influences source and properties of inflow to the Salish Sea and Columbia River Estuary. *Journal of Geophysical Research: Oceans*, *130*(2), e2024JC022024. https://doi.org/10.1029/2024JC022024

Broatch, E. M., & MacCready, P. (2022). Mixing in a salinity variance budget of the Salish Sea is controlled by river flow. *Journal of Physical Oceanography*, *52*(10), 2305–2323. https://doi.org/10.1175/JPO-D-21-0227.1

Burchard, H., Bolding, K., Feistel, R., Gräwe, U., Klingbeil, K., MacCready, P., et al. (2018). The Knudsen theorem and the total exchange flow analysis framework applied to the Baltic Sea. *Progress in Oceanography*, *165*, 268–286. https://doi.org/10.1016/j.pocean.2018.04.004

Burchard, H., & Hetland, R. D. (2010). Quantifying the contributions of tidal straining and gravitational circulation to residual circulation in periodically stratified tidal estuaries. *Journal of Physical Oceanography*, *40*(6), 1243–1262. https://doi.org/10.1175/2010JPO4270.1

Cannon, G. A., Holbrook, J. R., & Pashinski, D. J. (1990). Variations in the onset of bottom-water intrusions over the entrance sill of a fjord. *Estuaries*, *13*(1), 31–42. https://doi.org/10.2307/1351430

Chant, R. J. (2002). Secondary circulation in a region of flow curvature: Relationship with tidal forcing and river discharge. *Journal of Geophysical Research*, *107*(C9), 14-1–14-11. https://doi.org/10.1029/2001JC001082

Cloern, J. E., Foster, S. Q., & Kleckner, A. E. (2014). Phytoplankton primary production in the world's estuarine-coastal ecosystems. *Biogeosciences*, *11*(9), 2477–2501. https://doi.org/10.5194/bg-11-2477-2014

Cokelet, E. D., & Stewart, R. J. (1985). The exchange of water in fjords: The efflux/reflux theory of advective reaches separated by mixing zones. *Journal of Geophysical Research*, *90*(C4), 7287–7306. https://doi.org/10.1029/JC090iC04p07287

Davis, K. A., Banas, N. S., Giddings, S. N., Siedlecki, S. A., MacCready, P., Lessard, E. J., et al. (2014). Estuary-enhanced upwelling of marine nutrients fuels coastal productivity in the U.S. Pacific Northwest. *Journal of Geophysical Research: Oceans*, *119*(12), 8778–8799. https://doi.org/10.1002/2014JC010248

Deppe, R. W., Thomson, J., Polagye, B., & Krembs, C. (2018). Predicting deep water intrusions to Puget Sound, WA (USA), and the seasonal modulation of dissolved oxygen. *Estuaries and Coasts*, *41*(1), 114–127. https://doi.org/10.1007/s12237-017-0274-6

Du, J., Tepolt, C. K., Grason, E. W., Sean McDonald, P., Jia, Y., & Zhang, W. G. (2024). Dispersal pathways of European green crab larvae into and throughout the eastern Salish Sea. *Progress in Oceanography*, *223*, 103245. https://doi.org/10.1016/j.pocean.2024.103245

Engel, L., Premathilake, L., Barrier, N., Khangaonkar, T., & Garavelli, L. (2025). Larval connectivity for European green crab management in the Salish Sea and surrounding waters. *Marine Ecology Progress Series*, *754*, 77–92. https://doi.org/10.3354/meps14778

Feely, R. A., Sabine, C. L., Hernandez-Ayon, J. M., Ianson, D., & Hales, B. (2008). Evidence for upwelling of corrosive "Acidified" water onto the continental shelf. *Science*, *320*(5882), 1490–1492. https://doi.org/10.1126/science.1155676

Foreman, M. G. G., Callendar, W., MacFadyen, A., Hickey, B. M., Thomson, R. E., & Di Lorenzo, E. (2008). Modeling the generation of the Juan de Fuca Eddy. *Journal of Geophysical Research*, *113*(C3), C03006. https://doi.org/10.1029/2006JC004082

Foreman, M. G. G., Pal, B., & Merryfield, W. J. (2011). Trends in upwelling and downwelling winds along the British Columbia shelf. *Journal of Geophysical Research*, *116*(C10), C10023. https://doi.org/10.1029/2011JC006995

Frisch, A. S., Holbrook, J., & Ages, A. B. (1981). Observations of a summertime reversal in circulation in the Strait of Juan De Fuca. *Journal of Geophysical Research*, *86*(C3), 2044–2048. https://doi.org/10.1029/JC086iC03p02044

Garcia, A. M. P., & Geyer, W. R. (2023). Tidal dispersion in short estuaries. *Journal of Geophysical Research: Oceans*, *128*(2), e2022JC018883. https://doi.org/10.1029/2022JC018883

Geyer, W. R., & Cannon, G. A. (1982). Sill processes related to deep water renewal in a fjord. *Journal of Geophysical Research*, *87*(C10), 7985–7996. https://doi.org/10.1029/JC087iC10p07985

Geyer, W. R., & MacCready, P. (2014). The estuarine circulation. *Annual Review of Fluid Mechanics*, *46*(1), 175–197. https://doi.org/10.1146/annurev-fluid-010313-141302

Giddings, S. N., & MacCready, P. (2017). Reverse estuarine circulation due to local and remote wind forcing, enhanced by the presence of along-coast estuaries. *Journal of Geophysical Research: Oceans*, *122*(12), 10184–10205. https://doi.org/10.1002/2016JC012479

Giddings, S. N., MacCready, P., Hickey, B. M., Banas, N. S., Davis, K. A., Siedlecki, S. A., et al. (2014). Hindcasts of potential harmful algal bloom transport pathways on the Pacific Northwest coast. *Journal of Geophysical Research: Oceans*, *119*(4), 2439–2461. https://doi.org/10.1002/2013JC009622

Griffin, D. A., & LeBlond, P. H. (1990). Estuary/ocean exchange controlled by spring-neap tidal mixing. *Estuarine, Coastal and Shelf Science*, *30*(3), 275–297. https://doi.org/10.1016/0272-7714(90)90052-S

Hansen, D. V., & Rattray, M. (1965). Gravitational circulation in straits and estuaries. *Journal of Marine Research*, *23*, 104–122. Retrieved from https://digital.lib.washington.edu/server/api/core/bitstreams/238ceafe-4f97-4994-88b3-4997c952f71c/content

Harvey, M. E., Giddings, S. N., Pawlak, G., & Crooks, J. A. (2023). Hydrodynamic variability of an intermittently closed estuary over interannual, seasonal, fortnightly, and tidal timescales. *Estuaries and Coasts*, *46*(1), 84–108. https://doi.org/10.1007/s12237-021-01014-0

Hickey, B. M., Geier, S., Kachel, N., Ramp, S., Kosro, P. M., & Connolly, T. (2016). Alongcoast structure and interannual variability of seasonal midshelf water properties and velocity in the Northern California Current System. *Journal of Geophysical Research: Oceans*, *121*(10), 7408–7430. https://doi.org/10.1002/2015JC011424

Hickey, B. M., Thomson, R. E., Yih, H., & LeBlond, P. H. (1991). Velocity and temperature fluctuations in a buoyancy-driven current off Vancouver Island. *Journal of Geophysical Research*, *96*(C6), 10507–10538. https://doi.org/10.1029/90JC02578

Hickey, B. M., Zhang, X., & Banas, N. (2002). Coupling between the California Current System and a coastal plain estuary in low river flow conditions. *Journal of Geophysical Research*, *107*(C10), 30-1–30-20. https://doi.org/10.1029/1999JC000160

Holbrook, J. R., & Halpern, D. (1982). Winter-time near-surface currents in the Strait of Juan de Fuca. *Atmosphere-Ocean*, *20*(4), 327–339. https://doi.org/10.1080/07055900.1982.9649149

Jackson, R. H., Lentz, S. J., & Straneo, F. (2018). The dynamics of shelf forcing in Greenlandic Fjords. *Journal of Physical Oceanography*, *48*(11), 2799–2827. https://doi.org/10.1175/JPO-D-18-0057.1

Jay, D. A., & Musiak, J. D. (1996). Internal tidal asymmetry in channel flows: Origins and consequences. In *Mixing in estuaries and coastal seas* (pp. 211–249). American Geophysical Union (AGU). https://doi.org/10.1029/CE050p0211

Juarez, B., Valle-Levinson, A., & Canestrelli, A. (2022). Mechanisms of estuarine salt-plug formation by an along-shelf buoyant current: A numerical model approach. *Journal of Geophysical Research: Oceans*, *127*(4), e2021JC017971. https://doi.org/10.1029/2021JC017971

Juarez, B., Valle-Levinson, A., & Li, C. (2020). Estuarine salt-plug induced by freshwater pulses from the inner shelf. *Estuarine, Coastal and Shelf Science*, *232*, 106491. https://doi.org/10.1016/j.ecss.2019.106491

Khangaonkar, T., Nugraha, A., Xu, W., & Balaguru, K. (2019). Salish Sea response to global climate change, sea level rise, and future nutrient loads. *Journal of Geophysical Research: Oceans*, *124*(6), 3876–3904. https://doi.org/10.1029/2018JC014670

Khangaonkar, T., Nugraha, A., Xu, W., Long, W., Bianucci, L., Ahmed, A., et al. (2018). Analysis of hypoxia and sensitivity to nutrient pollution in Salish Sea. *Journal of Geophysical Research: Oceans*, *123*(7), 4735–4761. https://doi.org/10.1029/2017JC013650

Klinck, J. M., O'Brien, J. J., & Svendsen, H. (1981). A Simple model of Fjord and coastal circulation interaction. *Journal of Physical Oceanography*, *11*(12), 1612–1626. https://doi.org/10.1175/1520-0485(1981)011⟨1612:ASMOFA⟩2.0.CO;2

Knudsen, M. (1900). Ein hydrographischer lehrsatz. *Annalen der Hydrographie und Maritimen Meteorologie*, *28*(7), 316–320.

Largier, J. L. (2023). Recognizing low-inflow estuaries as a common estuary paradigm. *Estuaries and Coasts*, *46*(8), 1949–1970. https://doi.org/10.1007/s12237-023-01271-1

Lemagie, E. P., Giddings, S. N., MacCready, P., Seaton, C., & Wu, X. (2022). Measuring estuarine total exchange flow from discrete observations. *Journal of Geophysical Research: Oceans*, *127*(10), e2022JC018960. https://doi.org/10.1029/2022JC018960

Lerczak, J. A., Geyer, W. R., & Chant, R. J. (2006). Mechanisms driving the time-dependent salt flux in a partially stratified estuary. *Journal of Physical Oceanography*, *36*(12), 2296–2311. https://doi.org/10.1175/JPO2959.1

Lorenz, M., Klingbeil, K., MacCready, P., & Burchard, H. (2019). Numerical issues of the Total Exchange Flow (TEF) analysis framework for quantifying estuarine circulation. *Ocean Science*, *15*(3), 601–614. https://doi.org/10.5194/os-15-601-2019

MacCready, P. (2011). Calculating estuarine exchange flow using isohaline coordinates. *Journal of Physical Oceanography*, *41*(6), 1116–1124. https://doi.org/10.1175/2011JPO4517.1

MacCready, P. (2023). Code and data for Salish exchange dynamics paper [Dataset]. *Zenodo*. https://doi.org/10.5281/zenodo.10206344

MacCready, P., & Geyer, W. R. (2010). Advances in estuarine physics. *Annual Review of Marine Science*, *2*(1), 35–58. https://doi.org/10.1146/annurev-marine-120308-081015

MacCready, P., & Geyer, W. R. (2024). Estuarine exchange flow in the Salish Sea. *Journal of Geophysical Research: Oceans*, *129*(1), e2023JC020369. https://doi.org/10.1029/2023JC020369

MacCready, P., Geyer, W. R., & Burchard, H. (2018). Estuarine exchange flow is related to mixing through the salinity variance budget. *Journal of Physical Oceanography*, *48*(6), 1375–1384. https://doi.org/10.1175/JPO-D-17-0266.1

MacCready, P., McCabe, R. M., Siedlecki, S. A., Lorenz, M., Giddings, S. N., Bos, J., et al. (2021). Estuarine circulation, mixing, and residence times in the Salish Sea. *Journal of Geophysical Research: Oceans*, *126*(2), e2020JC016738. https://doi.org/10.1029/2020JC016738

Mackas, D. L., & Harrison, P. J. (1997). Nitrogenous nutrient sources and sinks in the Juan de Fuca Strait/Strait of Georgia/Puget Sound Estuarine System: Assessing the potential for eutrophication. *Estuarine, Coastal and Shelf Science*, *44*, 1–21. https://doi.org/10.1006/ecss.1996.0110

Martin, W. D., & MacCready, P. (2011). Influence of large-scale tidal asymmetry on subtidal dynamics in the western Strait of Juan de Fuca. *Journal of Geophysical Research*, *116*(C2), C02009. https://doi.org/10.1029/2010JC006363

Masoud, M., & Pawlowicz, R. (2023). A Predictably intermittent rotationally modified gravity current in the Strait of Georgia. *Journal of Physical Oceanography*, *53*(1), 81–96. https://doi.org/10.1175/JPO-D-22-0047.1

Masson, D. (2006). Seasonal water mass analysis for the Straits of Juan de Fuca and Georgia. *Atmosphere-Ocean*, *44*(1), 1–15. https://doi.org/10.3137/ao.440101

Mohamedali, T., Roberts, M., Sackmann, B., & Kolosseus, A. (2011). Puget sound dissolved oxygen model nutrient load summary for 1999–2008. (11-03-057).

Pareja-Roman, L. F., & Chant, R. J. (2023). Effects of a changing climate on the physics of estuaries. In *Climate change and estuaries*. CRC Press.

Pawlowicz, R. (2002). Observations and linear analysis of sill-generated internal tides and estuarine flow in Haro Strait. *Journal of Geophysical Research*, *107*(C6), 9-1–9-13. https://doi.org/10.1029/2000JC000504

Pawlowicz, R., Hannah, C., & Rosenberger, A. (2019). Lagrangian observations of estuarine residence times, dispersion, and trapping in the Salish Sea. *Estuarine, Coastal and Shelf Science*, *225*, 106246. https://doi.org/10.1016/j.ecss.2019.106246

Payo-Payo, M., Bricheno, L. M., Dijkstra, Y. M., Cheng, W., Gong, W., & Amoudry, L. O. (2022). Multiscale temporal response of salt intrusion to transient river and ocean forcing. *Journal of Geophysical Research: Oceans*, *127*(3), e2021JC017523. https://doi.org/10.1029/2021JC017523

Rykaczewski, R. R., Dunne, J. P., Sydeman, W. J., García-Reyes, M., Black, B. A., & Bograd, S. J. (2015). Poleward displacement of coastal upwelling-favorable winds in the ocean's eastern boundary currents through the 21st century. *Geophysical Research Letters*, *42*(15), 6424–6431. https://doi.org/10.1002/2015GL064694

Salamena, G. G., Whinney, J. C., Heron, S. F., & Ridd, P. V. (2021). Internal tidal waves and deep-water renewal in a tropical fjord: Lessons from Ambon Bay, eastern Indonesia. *Estuarine, Coastal and Shelf Science*, *253*, 107291. https://doi.org/10.1016/j.ecss.2021.107291

Sanchez, R. (2025). Data for limits of ocean forcing data [Dataset]. *Zenodo*. https://doi.org/10.5281/zenodo.13119092

Sanchez, R., Straneo, F., Hughes, K., Barbour, P., & Shroyer, E. (2024). Relative roles of plume and coastal forcing on exchange flow variability of a Glacial Fjord. *Journal of Geophysical Research: Oceans*, *129*(6), e2023JC020492. https://doi.org/10.1029/2023JC020492

Shchepetkin, A. F., & McWilliams, J. C. (2005). The regional oceanic modeling system (ROMS): A split-explicit, free-surface, topography-following-coordinate oceanic model. *Ocean Modelling*, *9*(4), 347–404. https://doi.org/10.1016/j.ocemod.2004.08.002

Sobocinski, K. L., Harvell, C. D., Baloy, N. J. K., Broadhurst, G., Dethier, M. N., Flower, A., & Delaney, J. R. (2022). Urban seas as hotspots of stress in the Anthropocene ocean: The Salish Sea example. *Elementa: Science of the Anthropocene*, *10*(1), 00055. https://doi.org/10.1525/elementa.2022.00055

Soto-Riquelme, C., Pinilla, E., & Ross, L. (2023). Wind influence on residual circulation in Patagonian channels and fjords. *Continental Shelf Research*, *254*, 104905. https://doi.org/10.1016/j.csr.2022.104905

Stevens, S. W., Pawlowicz, R., & Allen, S. E. (2021). A Study of intermediate water circulation in the Strait of Georgia using tracer-based, Eulerian, and Lagrangian methods. *Journal of Physical Oceanography*, *51*(6), 1875–1893. https://doi.org/10.1175/JPO-D-20-0225.1

Stommel, H., & Farmer, H. (1953). Control of salinity in an estuary by a transition. *Journal of Marine Research*, *12*(1). Retrieved from https://elischolar.library.yale.edu/journal_of_marine_research/778

Stone, H. B., Banas, N. S., & MacCready, P. (2018). The effect of Alongcoast advection on Pacific Northwest shelf and slope water properties in relation to upwelling variability. *Journal of Geophysical Research: Oceans*, *123*(1), 265–286. https://doi.org/10.1002/2017JC013174

Stone, H. B., Banas, N. S., MacCready, P., Trainer, V. L., Ayres, D. L., & Hunter, M. V. (2022). Assessing a model of Pacific Northwest harmful algal bloom transport as a decision-support tool. *Harmful Algae*, *119*, 102334. https://doi.org/10.1016/j.hal.2022.102334

Sutherland, D. A., MacCready, P., Banas, N. S., & Smedstad, L. F. (2011). A model study of the Salish Sea estuarine circulation. *Journal of Physical Oceanography*, *41*(6), 1125–1143. https://doi.org/10.1175/2011JPO4540.1

Sutton, J. N., Johannessen, S. C., & Macdonald, R. W. (2013). A nitrogen budget for the Strait of Georgia, British Columbia, with emphasis on particulate nitrogen and dissolved inorganic nitrogen. *Biogeosciences*, *10*(11), 7179–7194. https://doi.org/10.5194/bg-10-7179-2013

Thomson, R. E. & Emery, W. J. (Eds.) (2014). *Data analysis methods in physical oceanography* (3rd ed.). Elsevier. https://doi.org/10.1016/B978-0-12-387782-6.01001-2

Thomson, R. E., & Krassovski, M. V. (2015). Remote alongshore winds drive variability of the California undercurrent off the British Columbia-Washington coast. *Journal of Geophysical Research: Oceans*, *120*(12), 8151–8176. https://doi.org/10.1002/2015JC011306

Thomson, R. E., Kulikov, E. A., Spear, D. J., Johannessen, S. C., & Peter Wills, W. (2020). A role for gravity currents in cross-sill estuarine exchange and subsurface inflow to the Southern Strait of Georgia. *Journal of Geophysical Research: Oceans*, *125*(4), e2019JC015374. https://doi.org/10.1029/2019JC015374

Thomson, R. E., Mihály, S. F., & Kulikov, E. A. (2007). Estuarine versus transient flow regimes in Juan de Fuca Strait. *Journal of Geophysical Research*, *112*(C9), C09022. https://doi.org/10.1029/2006JC003925

Valle-Levinson, A. (2008). Density-driven exchange flow in terms of the Kelvin and Ekman numbers. *Journal of Geophysical Research*, *113*(C4), C04001. https://doi.org/10.1029/2007JC004144

Wetz, M. S., Hales, B., Chase, Z., Wheeler, P. A., & Whitney, M. M. (2006). Riverine input of macronutrients, iron, and organic matter to the coastal ocean off Oregon, U.S.A., during the winter. *Limnology & Oceanography*, *51*(5), 2221–2231. https://doi.org/10.4319/lo.2006.51.5.2221

Xiong, J., MacCready, P., & Leeson, A. (2024). Impact of estuarine exchange flow on multi-tracer budgets in the Salish Sea. *ESS Open Archive*. https://doi.org/10.22541/essoar.172252837.71181115/v1

Xiong, J., Shen, J., Qin, Q., & Du, J. (2021). Water exchange and its relationships with external forcings and residence time in Chesapeake Bay. *Journal of Marine Systems*, *215*, 103497. https://doi.org/10.1016/j.jmarsys.2020.103497

Yamada, S. B., Gillespie, G. E., Thomson, R. E., & Norgard, T. C. (2021). Ocean indicators predict range expansion of an introduced species: Invasion history of the European Green Crab Carcinus maenas on the North American Pacific Coast. *Journal of Shellfish Research*, *40*(2), 399–413. https://doi.org/10.2983/035.040.0212

Yamada, S. B., Thomson, R. E., Gillespie, G. E., & Norgard, T. C. (2017). Lifting barriers to range expansion: The European Green Crab Carcinus maenas (Linnaeus, 1758) enters the Salish Sea. *Journal of Shellfish Research*, *36*(1), 201–208. https://doi.org/10.2983/035.036.0121